




Electronic specific heat coefficient and magnetic properties of $Y(Fe_{1-x}Co_x)_2$ Laves phases: A combined experimental and first-principles study

Bartosz Wasilewski, Zbigniew Śniadecki , and Mirosław Werwiński *

Institute of Molecular Physics, Polish Academy of Sciences, ul. M. Smoluchowskiego 17, 60-179 Poznań, Poland

Natalia Pierunek

*Faculty of Physics, Adam Mickiewicz University, Uniwersytetu Poznańskiego 2, 61-614 Poznań, Poland
and Institute of Molecular Physics, Polish Academy of Sciences, ul. M. Smoluchowskiego 17, 60-179 Poznań, Poland*

Ján Rusz and Olle Eriksson 

Department of Physics and Astronomy, Uppsala University, Box 516, SE-751 20 Uppsala, Sweden



(Received 9 August 2019; revised manuscript received 8 October 2019; published 30 October 2019)

We investigated experimentally and computationally the concentration dependence of the electronic specific heat coefficient γ in the $Y(Fe_{1-x}Co_x)_2$ pseudobinary Laves phase system. The experimentally observed maximum in $\gamma(x)$ around the magnetic phase transition was interpreted within the local density approximation combined with the virtual crystal approximation. To explain the formation of the observed maximum, we analyzed theoretically the dependence of the magnetic energy, magnetic moments, densities of states, and Fermi surfaces on the Co concentration. Furthermore, we carried out the calculations of the density of states (DOS) at the Fermi level as a function of fixed spin moment. The calculated Co concentration at which γ takes the maximum value ($x_{\text{max-LDA-VCA}} = 0.91$) stays in good agreement with the measured value ($x_{\text{max-expt}} = 0.925$). We conclude that the observed maximum in $\gamma(x)$ results from the presence of the sharp DOS peak in the vicinity of the Fermi level.

DOI: [10.1103/PhysRevB.100.134436](https://doi.org/10.1103/PhysRevB.100.134436)

I. INTRODUCTION

The Laves phases are the largest group of intermetallic compounds [1]. They crystallize in close-packed structure classified into three types: Hexagonal $MgZn_2$ (C14), cubic $MgCu_2$ (C15), and hexagonal $MgNi_2$ (C36) [2–4]. The $Y(Fe_{1-x}Co_x)_2$ alloys crystallize in the cubic C15 $MgCu_2$ -type structure [5] with the space group $Fd-3m$ (No. 227); see Fig. 1 and Table I. The primitive cell of YCo_2 consists of two Y and four Co atoms. The sublattice of Y has a diamond structure and the sublattice of Co forms the kagome lattice (trihexagonal tiling). YFe_2 is a ferromagnet with the Curie temperature of about 550 K [6,7], while YCo_2 is an exchange-enhanced Pauli paramagnet [8] undergoing a metamagnetic transition in a field of about 70 T (at 10 K) [9,10]. Fe/Co alloying induces a paramagnetic-ferromagnetic phase transition in the $Y(Fe, Co)_2$ system with a critical Fe concentration of about 0.14 [11]. The measured dependence of magnetic moment (m) on Co concentration starts at $2.80 \mu_B \text{ f.u.}^{-1}$ for YFe_2 , reaches a broad maximum for intermediate concentrations, and drops sharply to zero near the critical Co concentration [11]. The pseudobinary Laves phases $Y(Fe_{1-x}Co_x)_2$ exhibit both extraordinary magnetic properties [7,12–15] and the ability to absorb hydrogen [16–19]. Moreover, the $DyFe_2/YFe_2$ magnetic thin films are reversible exchange-spring magnets [20,21] and the YCo_2 alloys with rare-earth elements

$R_{1-x}Y_xCo_2$ ($R = Er, Gd$) are considered as magnetocaloric materials for application in magnetic refrigerators [22,23].

Our previous experimental and theoretical investigations on the $Y(Fe_{1-x}Co_x)_2$ system covered such issues as the magnetic moments of $Y(Fe_{1-x}Co_x)_2$ [24,25], electronic structure of YCo_2 [26,27], effect of YCo_2 doping [28], magnetic percolation in $Y(Fe_{1-x}Co_x)_2$ [29], Curie temperature of $Y(Fe_{1-x}Co_x)_2$ [30], and structural disorder in YCo_2 [31].

In this work we focus on the concentration dependence of the electronic specific heat coefficient γ , where the specific heat is a temperature derivative of the internal energy. The temperature dependence of specific heat consists of a lattice contribution and linear electronic term γT . As the Fermi-Dirac statistic indicates, only a small fraction of electrons contributes to the specific heat and the electronic contribution is the most pronounced in metals at low temperatures. In the Sommerfeld model, the electronic specific heat coefficient γ is calculated by converting the value of the density of states at the Fermi level [$DOS(E_F)$] according to the equation

$$\gamma = \frac{1}{3}\pi^2 k_B^2 DOS(E_F), \quad (1)$$

where k_B is the Boltzmann constant [32].

II. EXPERIMENTAL AND COMPUTATIONAL DETAILS

The ingots of several $Y(Fe_{1-x}Co_x)_2$ compositions ($x = 0.85, 0.90, 0.925, 0.95, \text{ and } 0.985$) were prepared with the use of arc furnace by repeated melting of required amounts of high-purity Y (99.9%), Co (99.9%), and Fe (99.9%) in Ar

*Corresponding author: werwinski@ifmpan.poznan.pl

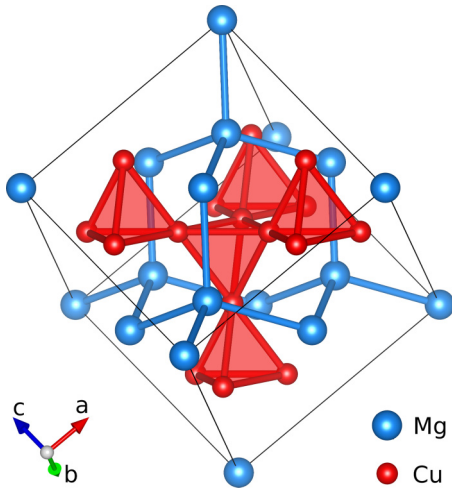


FIG. 1. Crystal structure of the cubic MgCu_2 -type Laves phase.

atmosphere. The polycrystalline master alloys were rapidly quenched in a melt-spinning device on a rotating copper wheel with the surface velocity of 40 m s^{-1} . The x-ray diffraction with Co K_α radiation in Bragg-Brentano geometry was used to characterize the crystalline structure of the melt-spun flakes. The temperature dependencies of heat capacity were measured with the two-tau relaxation method using the Quantum Design Physical Property Measurement System.

To simulate the chemical disorder in the theoretical models of the considered $\text{Y}(\text{Fe}_{1-x}\text{Co}_x)_2$ alloys three different methods were used: The coherent potential approximation (CPA) [33,34], the virtual crystal approximation (VCA) [25], and the ordered compound method (also called the supercell method) [24]. The density functional theory (DFT) calculations were conducted with the full-potential local-orbital scheme (FPLO) [35]. The older FPLO5.00-18 version of the code was used for the CPA, which is not available in the more recent versions. The rest of the calculations were performed with the FPLO14.0-49. For the exchange-correlation potential, we used the Perdew and Wang (PW92) model of the local-spin-density approximation [36]. As a result of using the CPA, we had to limit our calculations to the scalar-relativistic approximation. This is because in the FPLO5.00-18 version of the code, the CPA calculation can only be carried out with the scalar-relativistic approximation (not including spin-orbit coupling); therefore for consistency this approach was also used in other cases. The calculations were done using a $40 \times 40 \times 40$ \mathbf{k} mesh for the VCA and $16 \times 16 \times 16$ \mathbf{k} mesh for the CPA and ordered compound methods. For all three approaches we used the criterion of simultaneous energy and density convergence with an accuracy of $\sim 2.72 \times 10^{-7}$ eV (10^{-8} Ha) and 10^{-6} , respectively. In the FPLO5 the Y(4s, 4p)

TABLE I. Atomic coordinates for YFe_2 and YCo_2 , space group $Fd-3m$ (No. 227), origin choice two.

atom	site	x	y	z
Y	8(a)	1/8	1/8	1/8
Fe/Co	16(d)	1/2	1/2	1/2

and Fe/Co(3s, 3p) electrons were treated as semicore with the Y 4s and 4p orbitals having separate compression parameters, while the 3s and 3p orbitals in Fe and Co have a joint one. The Y(5s, 5p, 4d) and Fe/Co(4s, 4p, 3d) electrons were treated as valence ones. The considered crystallographic models were based on the optimized lattice parameters, as the application of the experimental parameters for YCo_2 resulted in a ferromagnetic ground state, which is not consistent with the empirical data [27,31,37]. Due to the overbinding nature of the local density approximation (LDA), the calculated lattice parameters (7.05 Å for YFe_2 and 6.95 Å for YCo_2) are much smaller than the experimental ones (7.36 Å for YFe_2 and 7.22 Å for YCo_2 [7]). However, they stay in good agreement with the previous LDA results (7.04 Å for YFe_2 and 6.96 Å for YCo_2 [37,38]). The lattice parameters for the intermediate $\text{Y}(\text{Fe}_{1-x}\text{Co}_x)_2$ concentrations were interpolated assuming a linear behavior of $a(x)$ dependence, which is in good agreement with experiment [7]. In case of the ordered compound approach, we started with a model of the YFe_2 supercell, composed of two primitive cells including four Y atoms and eight Fe atoms. We consequently substituted Fe by Co in the Y_4Fe_8 master cell producing a series of ordered ternary compounds: $\text{Y}_4\text{Fe}_7\text{Co}_1$, $\text{Y}_4\text{Fe}_6\text{Co}_2$, $\text{Y}_4\text{Fe}_5\text{Co}_3$, etc. The detailed crystallographic data of these compounds are summarized in Table III of the Appendix. The VESTA code [39] was used for visualization of the crystal structure.

We determined the enhanced specific heat coefficients $\gamma_{\text{calc-enh}}$ by multiplying the γ values calculated from Eq. (1) by the so called enhancement factor ($\tilde{\gamma}$). For each considered composition we used a single value of enhancement factor $\tilde{\gamma}$ equal to 6.87, which has been obtained by Tanaka and Harima for YCo_2 by adjusting the γ_{calc} to γ_{expt} [45]. Tanaka and Harima have introduced the enhancement factor motivating that for the strongly correlated electron systems the many-body effects can be taken into account considered as self-energy of the Co d electrons [45]. The enhancement factor ($\tilde{\gamma}$) was expressed as an energy derivative of the self-energy [$\Sigma(\omega)$],

$$\tilde{\gamma} = 1 - \{\partial \Sigma(\omega) / \partial \omega\}_{\omega=E_F}, \quad (2)$$

where $\Sigma(\omega)$ was calculated with the method of second-order perturbation for Coulomb interactions (U_{dd}) between Co d electrons in the framework of the Fermi liquid theory on the basis of a periodic Anderson model. The value of $\tilde{\gamma} = 6.87$ has been obtained by Tanaka and Harima by assuming U_{dd} equal 1.8 eV [45]. Details of this method can be found in Ref. [46] along with examples of applications.

III. RESULTS AND DISCUSSION

A. Experimental results and discussion

The experimental study of $\gamma(x)$ is conducted in the vicinity of Co concentration $x = 0.9$, where the maximum in γ has been previously observed [40]. However, the foregoing study has been carried out with a relatively large step of $\Delta x = 0.1$. Our results of specific heat (C_p) measurements in a temperature range between 2 and 70 K are presented in the inset of Fig. 2. The $C_p(T)$ curves do not show any apparent differences and no indication of a long-range magnetic ordering is visible in the plots. However, the C_p/T versus T^2 dependencies

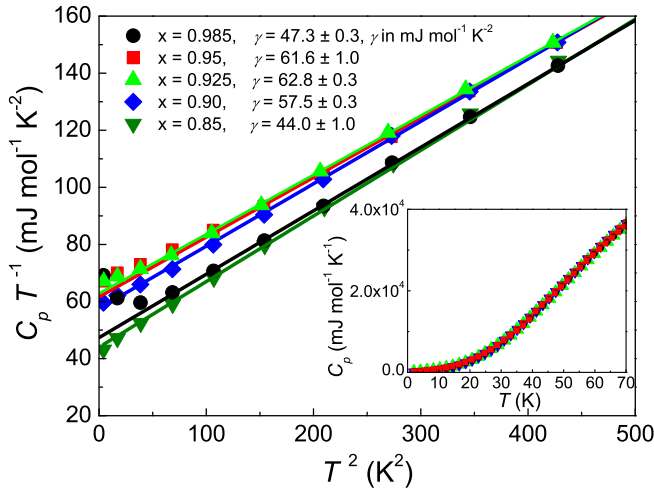


FIG. 2. The C_p/T versus T^2 dependencies for several $Y(\text{Fe}_{1-x}\text{Co}_x)_2$ compositions, where $x = 0.85, 0.90, 0.925, 0.95,$ and 0.985 . The symbols denote the experimental results, while the solid lines denote the fitting. Inset shows the temperature dependencies of the specific heat (C_p).

already reveal how the γ coefficient changes with x . The concentration dependence of the Sommerfeld coefficient exhibits a broad peak with the maximum of $62.8 \text{ mJ mol}^{-1} \text{ K}^{-2}$ at $x = 0.925$; see Fig. 3 and Table II. This result is in a good agreement with the previous one indicating the γ_{max} slightly below $60 \text{ mJ mol}^{-1} \text{ K}^{-2}$ located at $x = 0.9$ [40].

For x equal to $0.925, 0.95,$ and 0.985 , the estimations of γ_{expt} were done excluding nonlinear low-temperature regions. Nonlinearity, in the form of a significant upturn on the $C_p/T(T^2)$ dependence, is visible at low temperatures for $x = 0.985$ in the inset of Fig. 2. Some deviations from linearity were also detected for $x = 0.925$ and 0.95 . For $x = 0.85$ and 0.90 the linear dependencies in $C_p/T(T^2)$ were measured down to the lowest temperatures. A very small upturn of $C_p/T(T^2)$ for $x = 0.925$ suggests that this alloy is just below the critical concentration for magnetic percolation. A similar anomaly has been also observed for other Laves phases, as for example for $Y_{1-x}\text{Gd}_x\text{Co}_2$ [41]. Thus, being careful one can determine the critical concentration as $0.90 < x_{\text{crit}} < 0.95$, with the other authors reporting somewhat lower values, $x_{\text{crit}} \sim 0.86$ [11], 0.88 [42], and 0.895 [42]. The shift

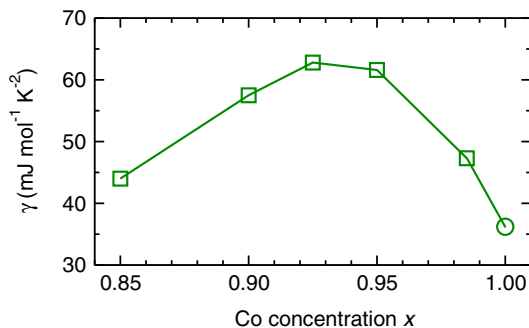


FIG. 3. The experimental electronic specific heat coefficient γ as measured for $Y(\text{Fe}_{1-x}\text{Co}_x)_2$ system. The value of γ for YCo_2 ($x = 1.0$) comes from Muraoka *et al.* [40].

TABLE II. The experimental electronic specific heat coefficient γ_{expt} , in $\text{mJ mol}^{-1} \text{ K}^{-2}$, measured for $Y(\text{Fe}_{1-x}\text{Co}_x)_2$ system in the Co-rich region ($0.85 \leq x \leq 0.985$). Δ is an estimated error of the measured value.

	$x = 0.85$	0.90	0.925	0.95	0.985
γ_{expt}	44.0	57.5	62.8	61.6	47.3
Δ	± 1.0	± 0.3	± 0.3	± 1.0	± 0.3

of the measured critical concentration can be explained as an effect of using the rapid quenching technique for synthesis of our alloys. This results in chemical and topological disorder being introduced, which leads to the formation of the magnetically ordered state [28,29,31]. When starting from an exchange-enhanced Pauli paramagnet YCo_2 , an introduction of structural disorder (or addition of other element) causes the formation of magnetically ordered clusters (spin-glass-type behavior) with nonzero magnetic moment on Co atoms. Formation of such magnetic clusters has been described for $Y_{1-x}\text{Gd}_x\text{Co}_2$ as a “microscopic” metamagnetic phase transition that occurs at a sufficiently high molecular field acting on Co atoms [41]. Magnetic percolation to the long-range magnetic ordering takes place when the volume and number of magnetic clusters, which can be described as localized spin density fluctuations, are increasing. Such fluctuations originate from the distribution of d - d exchange coupling due to the presence of chemical or structural disorder and from the inhomogeneous distribution of the local density of states. This picture leads to the conclusion that the additional contribution to the heat capacity of the samples above x_{crit} is connected with the presence of magnetically ordered clusters. The above suggests a close connection between the maximum in $\gamma(x)$ and magnetic phase transition in the considered Laves phases.

TABLE III. Crystallographic data for $Y_4\text{Fe}_7\text{Co}_1$, $Y_4\text{Fe}_6\text{Co}_2$, $Y_4\text{Fe}_5\text{Co}_3$, and $Y_4\text{Fe}_4\text{Co}_4$ ordered compounds, where a is the cubic Laves phase lattice parameter (optimized a equals 7.045 \AA for YFe_2 and 6.95 \AA for YCo_2 ; s.g. = space group).

$Y_4\text{Fe}_7\text{Co}_1$ s.g. 20 C222 ₁					$Y_4\text{Fe}_5\text{Co}_3$ s.g. 20 C222 ₁				
$a, b, c:$	$a\sqrt{2}$	$a\sqrt{2}$	a		$a, b, c:$	$a\sqrt{2}$	$a\sqrt{2}$	a	
atom	x	y	z		atom	x	y	z	
1	Y	1/8	1/8	1/8	1	Y	3/8	7/8	1/8
2	Y	1/8	3/8	7/8	2	Y	7/8	1/8	7/8
3	Fe	1/2	1/8	3/4	3	Fe	1/2	3/8	3/4
4	Fe	3/8	1/4	0	4	Fe	5/8	1/4	0
5	Fe	3/4	1/8	3/4	5	Fe	1/4	3/8	3/4
6	Fe	5/8	0	1/2	6	Co	7/8	0	1/2
7	Fe	1/2	3/8	1/4	7	Co	1/2	1/8	1/4
8	Co	1/8	0	1/2	8	Co	3/8	0	1/2
$Y_4\text{Fe}_6\text{Co}_2$ s.g. 213 P4 ₁ 32					$Y_4\text{Fe}_4\text{Co}_4$ s.g. 91 P4 ₁ 22				
$a, b, c:$	a	a	a		$a, b, c:$	$a/\sqrt{2}$	$a/\sqrt{2}$	a	
atom	x	y	z		atom	x	y	z	
1	Y	0	1/2	1/2	1	Y	3/4	3/4	7/8
2	Co	3/8	3/8	3/8	2	Fe	1/4	0	3/4
3	Fe	7/8	7/8	3/8	3	Co	3/4	1/2	1/4

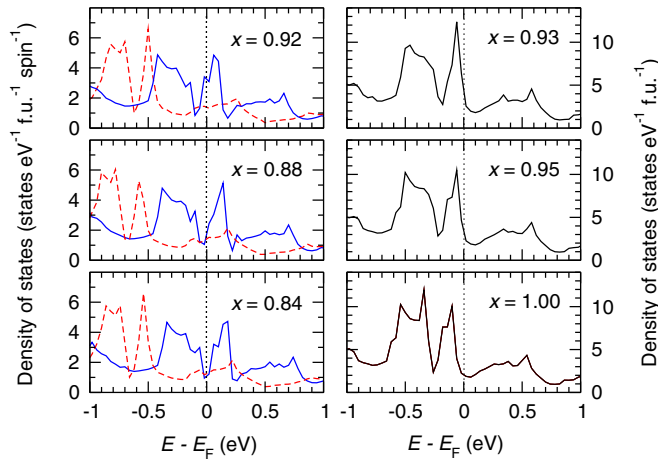


FIG. 4. To analyze the formation of the maximum in $\gamma(x)$ on the Co-rich region of the $Y(\text{Fe}_{1-x}\text{Co}_x)_2$ system, we employed the local density approximation (LDA) in combination with the virtual crystal approximation (VCA). Here we show the calculated (with LDA-VCA) densities of states for Co concentrations near $x_{\text{crit}} \sim 0.925$ at which a ferromagnetic-nonmagnetic phase transition occurs in the $Y(\text{Fe}_{1-x}\text{Co}_x)_2$ system. Results of spin-polarized calculations are presented on the left, with solid lines denoting majority and dashed lines denoting minority spin channels. The nonmagnetic results are shown on the right.

B. Theoretical results and discussion

According to Muraoka *et al.* [40] the characteristic enhancement of $\gamma(x)$ around the critical concentration should be attributed to the spin fluctuations. Subsequently, two theoretical attempts have been made by Shimizu *et al.* to reproduce the maximum in $\gamma(x)$ [43,44]. The first approach was based on the Green's functions method [43] and in the second one the rigid-band model was used on top of the YCo_2 density of states (DOS) from the tight-binding approximation [44]. Unfortunately, the $\gamma(x)$ dependencies obtained from both methods are unsatisfactory, especially in the vicinity of the magnetic transition.

1. Densities of states and electronic specific heat coefficient

In Fig. 4 we present the densities of states for several Co-rich compositions of the $Y(\text{Fe}_{1-x}\text{Co}_x)_2$ system. A comparison of total energies of ferromagnetic and nonmagnetic ground-state solutions indicates a magnetic phase transition at $x_{\text{crit}} \sim 0.925$. The presented DOSs are spin polarized for a ferromagnetic region ($x < 0.925$) and nonmagnetic above the critical concentration ($x > 0.925$). The valence bands of the considered alloys start at about -7 eV with the most significant contributions from the $3d$ states located above -4 eV [31,45]. The DOS plots presented in Fig. 4 cover only the narrow region between -1 and 1 eV, which is the most important from the perspective of magnetic phase transition. For YCo_2 we observe a characteristic sharp peak near the Fermi level (E_F). A decrease of Co concentration leads to the depopulation of the valence band, whereby the relative position of the Fermi level moves toward the center of that peak. Due to the exchange interactions that peak splits asymmetrically below the critical concentration

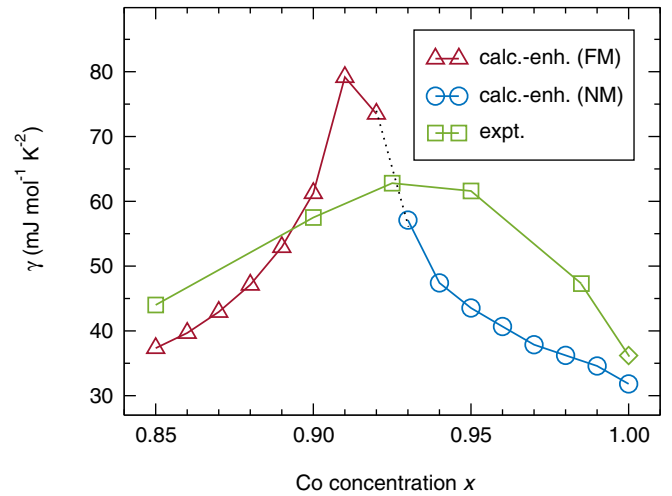


FIG. 5. The calculated (with LDA-VCA) enhanced electronic specific heat coefficient $\gamma_{\text{calc-enh}}$ for the $Y(\text{Fe}_{1-x}\text{Co}_x)_2$ system in the Co-rich region ($0.85 \leq x < 1$), together with the experimental dependence of γ_{expt} . The enhancement factor $\tilde{\gamma} = 6.87$ was applied as calculated for YCo_2 by Tanaka and Harima [45]. The $\gamma_{\text{calc-enh}}$ plot consists of two sections, ferromagnetic (FM) and nonmagnetic (NM), on the two sides of the phase transition determined by $x_{\text{crit}} \sim 0.925$. The value of γ for YCo_2 ($x = 1.0$) comes from Muraoka *et al.* [40].

($x_{\text{crit}} \sim 0.925$). The majority spin channel (the occupied one, red in Fig. 4) moves toward lower energies by about 0.4 eV, while the minority spin channel (the unoccupied one, blue) is shifted toward higher energies by about 0.2 eV. Since the sharp peak of the minority spin channel is located on the Fermi level, the DOS at the Fermi level increases. Further decrease in Co concentration leads to an increase of the magnetic moment and thus to increase of the exchange splitting. That shifts the observed sharp peak below the Fermi level toward the higher energies and the DOS at the Fermi level decreases.

In the next step we calculate the values of γ from $\text{DOS}(E_F)$ according to Eq. (1). For the nonmagnetic YCo_2 ($x = 1.00$) the γ_{calc} is equal to $4.6 \text{ mJ mol}^{-1} \text{ K}^{-2}$ and it is relatively close to a previously calculated value equal to $6.1 \text{ mJ mol}^{-1} \text{ K}^{-2}$ [45]. Both of those calculated values are distant from the experimental one, equal to $36.2 \text{ mJ mol}^{-1} \text{ K}^{-2}$ (per mole of YCo_2) [40]. The underestimation of γ values is a recognized DFT weakness related to disregard of spin fluctuations and many-body effects in low-energy excitations [45]. The many-body effects can be taken into account by considering the self-energy of the correlated electrons. By using that approach Tanaka *et al.* justified the introduction of the so called enhancement factor ($\tilde{\gamma}$) [45,46]; see Sec. II for more details. The enhancement factor for YCo_2 , obtained by Tanaka and Harima by adjusting the calculated values of the specific heat coefficient to the experimental value, is equal to 6.87 [45]. We use this single value to calculate the enhanced specific heat coefficient ($\gamma_{\text{calc-enh}}$) for each considered composition simply by multiplying the calculated with LDA specific heat coefficient γ_{calc} by the enhancement factor $\tilde{\gamma} = 6.87$. The $\gamma_{\text{calc-enh}}(x)$ dependence consists of two regions (ferromagnetic and nonmagnetic) separated by a phase transition at $x_{\text{crit}} \sim 0.925$; see Fig. 5. Similarly to the

experimental result it shows a maximum for the Co-rich compositions close to x_{crit} . The calculated and experimental Co concentrations for which the maximum in γ is observed are in good agreement with each other ($x_{\text{max-LDA-VCA}} = 0.91$ and $x_{\text{max-expt}} \sim 0.925$). The shape of the $\gamma_{\text{calc-enh}}(x)$ dependence results directly from the contour of a narrow peak observed about 0.1 eV below E_F in the DOS plot of YCo_2 ; see Fig. 4. The position of this peak in relation to E_F changes with x and for the Co concentration range between about 0.85 and 1.00 this peak is fully scanned by the E_F which is reflected in the observed maximum in $\text{DOS}(E_F)(x)$ and further in the corresponding $\gamma_{\text{calc-enh}}(x)$ dependence.

The calculated (without enhancement) maximum of the specific heat coefficient γ_{max} is around $12 \text{ mJ mol}^{-1} \text{ K}^{-2}$ (at $x_{\text{max}} = 0.91$). This value multiplied by the enhancement parameter ($\tilde{\gamma} = 6.87$) gives the maximum of enhanced specific heat coefficient $\gamma_{\text{max-enh}} \sim 70 \text{ mJ mol}^{-1} \text{ K}^{-2}$, whereas the experimental value $\gamma_{\text{max-expt}}$ is around $62.8 \text{ mJ mol}^{-1} \text{ K}^{-2}$ [per mole of $\text{Y}(\text{Fe}_{0.075}\text{Co}_{0.925})_2$] for $x = 0.925$; see Table II. The cause of this big difference between the γ_{max} and $\gamma_{\text{max-expt}}$, besides the disregard of many-body effects, can be due to not taking into account the additional impact of spin fluctuations around the magnetic phase transition in the theoretical models [40]. The enhanced specific heat coefficient $\gamma_{\text{max-enh}}$ is much closer to $\gamma_{\text{max-expt}}$, but at the price of using the enhancement parameter $\tilde{\gamma}$ justified by the model considering many-body effects but still neglecting spin fluctuations [45,46].

It is a little bit surprising that the calculated peak of γ does not coincide with the $x_{\text{crit-LDA-VCA}} \sim 0.925$, but instead occurs at $x_{\text{max}} = 0.91$. Unfortunately, the results of our measurements ($x_{\text{max}} \sim 0.925$ and $0.90 < x_{\text{crit}} < 0.95$) are not accurate enough to confirm this effect in $\text{Y}(\text{Fe}_{1-x}\text{Co}_x)_2$. However, a much larger difference has been previously measured for the $\text{Zr}(\text{Fe}_{1-x}\text{Co}_x)_2$ system, with $x_{\text{max}} = 0.5$ and $x_{\text{crit}} = 0.75$ [47].

The observed discrepancies between the experimental and computational results of $\gamma(x)$ arise, among other things, from not considering many-body effects and spin fluctuations in the theoretical description. They can be also partly attributed to the shortcomings of the LDA and VCA. The application of the LDA results in reduction of the lattice parameter due to overbinding, and it is accompanied by reduction of the magnetic moments, underestimation of the magnetic energy, and shift of the critical Co concentration for which the magnetic transition occurs, whereas the VCA simplifies the nature of chemical disorder by forming a homogeneous crystal. As a result, we received a sharp band structure without any broadening coming from the chemical disorder, which is observed in the angle-resolved photoemission spectroscopy (ARPES) measurements and in the CPA calculations of disordered alloys. So why did we choose the VCA instead of the CPA to do the research? An application of the CPA would not allow us to analyze the fixed spin moment and Fermi surface, which results will be presented in the following sections. Nevertheless, we have also performed the additional CPA-LDA calculations, which have confirmed the presence of the magnetic phase transition and the maximum in $\gamma(x)$ for the Co-rich compositions. However, the CPA maximum in $\gamma(x)$ is much smoother than that from the VCA method, which can be related to the mentioned broadening caused by chemical

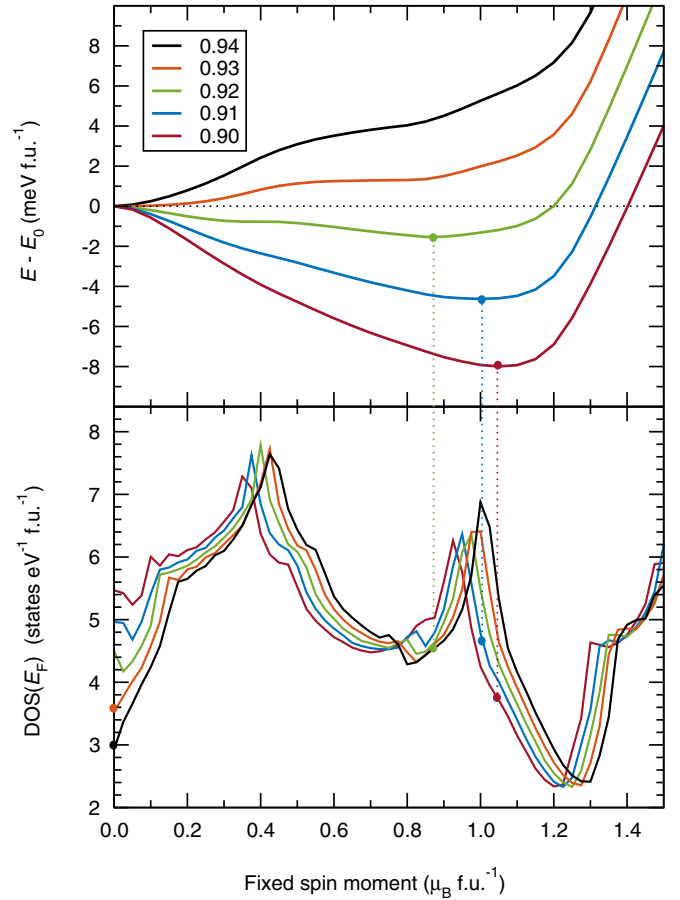


FIG. 6. The calculated (with LDA-VCA method) magnetic energy and density of states at Fermi level versus fixed spin moment for several Co concentrations in the vicinity of the critical concentration $x_{\text{crit}} \sim 0.925$ at which occurs a ferromagnetic-nonmagnetic phase transition for the $\text{Y}(\text{Fe}_{1-x}\text{Co}_x)_2$ system. The ground states $\text{DOS}(E_F)$ are marked with colored dots. The vertical dashed lines connect the magnetic energy minima with corresponding $\text{DOS}(E_F)$.

disorder. Some results of the CPA calculations will be also presented in the further part of the study.

2. Fixed spin moment calculations

The fixed spin moment (FSM) method allows for calculations of the systems with a nonequilibrium magnetic moment, and hence it enables us to plot the magnetic energy dependence as a function of spin magnetic moment [9], where the magnetic energy is the energy difference between the magnetic and nonmagnetic ground state solutions. The FSM calculations have already helped to understand the magnetic behavior of YCo_2 [9,27]. We performed a series of FSM calculations for several successive concentrations near the magnetic transition of the $\text{Y}(\text{Fe}_{1-x}\text{Co}_x)_2$ system; see Fig. 6. The presented dependencies of magnetic energy and the density of states at the Fermi level [$\text{DOS}(E_F)$] on the FSM are intended to explain the behavior of $\gamma(x)$. In order to obtain accurate plots of $\text{DOS}(E_F)$ versus FSM, it was necessary to use a very small step in FSM ($0.025 \mu_B$). The magnetic energy plots, in the top panel, confirm that within the LDA-VCA the magnetic phase transition in $\text{Y}(\text{Fe}_{1-x}\text{Co}_x)_2$ occurs at Co

concentration equal to about 0.925. The plots show minima for nonzero moments above this value. The positions of the minima shift toward higher magnetic moments with a decrease of Co concentration, wherein the deeper the minimum, the more stable the ferromagnetic state is. The overall shape of $\text{DOS}(E_F)(m)$ is similar for all considered Co concentrations. The observed double-peak structure is related to the DOS plot with the characteristic maximum near the Fermi level. The observed shift of the $\text{DOS}(E_F)(m)$ plots toward the higher magnetic moments for increasing Co concentration x comes from filling of the electronic band structure of $\text{Y}(\text{Fe}_{1-x}\text{Co}_x)_2$ after alloying with the element possessing more valence electrons. The minima in magnetic energies clearly correspond with the ground state values of $\text{DOS}(E_F)$. When we look at the values of the ground state $\text{DOS}(E_F)$ for subsequent Co concentrations, we observe the change of tendencies, leading to the formation of the maximum in $\text{DOS}(E_F)$ versus x , and thus in the considered dependence of $\gamma(x)$. It gives another perspective for understanding of the formation of maximum in $\gamma(x)$.

3. Fermi surface

Another insight into the nature of the electronic specific heat coefficient γ can be achieved from the perspective of the Fermi surface. As we discussed in Sec. I, γ is directly estimated from $\text{DOS}(E_F)$, where the latter is obtained by integration of the states on the Fermi level over the whole Brillouin zone. A distribution of the states at the Fermi level in the first Brillouin zone is called the Fermi surface. Thus, the observed maximum in γ correlates with the largest area of the Fermi surface, as presented in Fig. 7 for several successive Co concentrations. The Fermi surfaces presented in the right column are nonmagnetic solutions, while the ones shown in the left column are spin polarized.

The nonmagnetic Fermi surface for the terminal concentration $x = 1.00$ (YCo_2) consists of three sheets. The electron-type surface, denoted with red color, is centered at the high-symmetry point X and consists of rectangular parts connected at W points. The other two surfaces are of the hole type and are located around the Γ point. One of them is nested and thus not visible in the figure. The Fermi surface calculated for YCo_2 is consistent with the previous theoretical results [46]. We suspect that the small differences observed around the W point may come from the various forms of the LDA exchange-correlation potential used in the compared models or from the inclusion of the spin-orbit interactions in the previous model [46].

An evolution of the Fermi surface is observed with decrease of the Co concentration ($x = 0.95$ and 0.93). The new features are forming around the W point. The hole-type surfaces (blue color) are enlarging, which leads to an increase of $\text{DOS}(E_F)$ and eventually to fulfillment of the Stoner criterion at $x_{\text{crit}} \approx 0.925$. The decrease of x leads to a magnetic phase transition, which also manifests in the shape of the Fermi surfaces. The spin-polarized Fermi surface for $x = 0.92$ consists of two overlapping spin channels and has the largest area of all Fermi surfaces shown in Fig. 7. The characteristic feature of the spin-polarized solutions is the hole-type nested double tubes along the Γ - L direction. The Fermi surfaces for even lower Co concentrations ($x = 0.88$ and 0.84) exhibit a

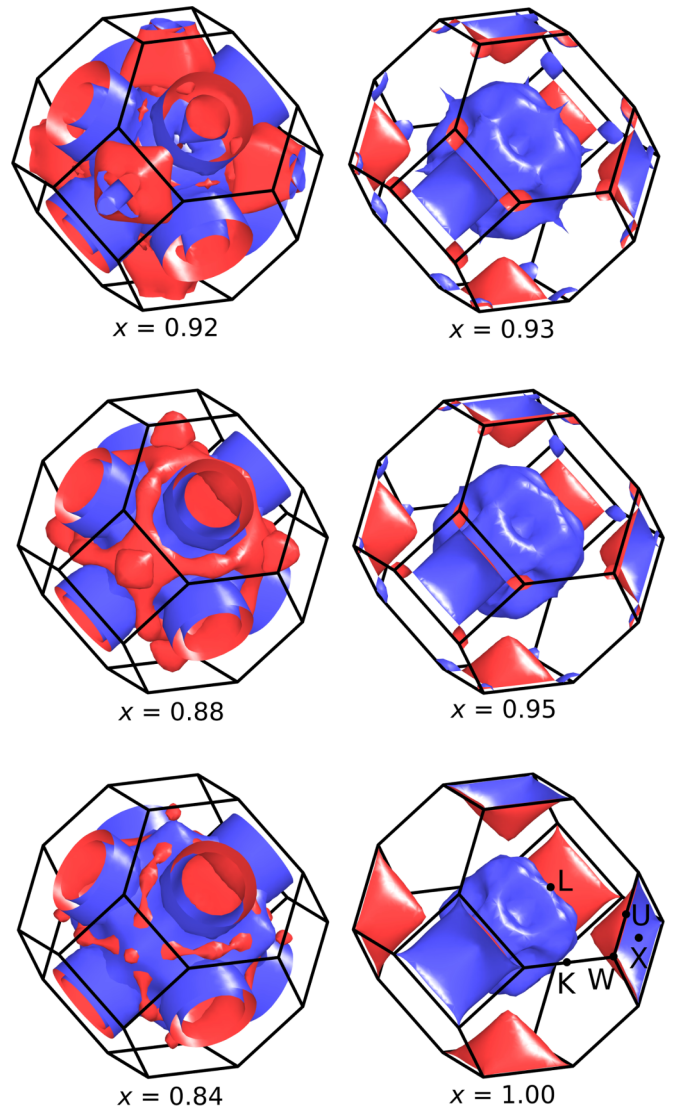


FIG. 7. The Fermi surfaces of $\text{Y}(\text{Fe}_{1-x}\text{Co}_x)_2$ calculated within LDA-VCA in the vicinity of the critical concentration $x_{\text{crit}} \sim 0.925$ at which the ferromagnetic-nonmagnetic phase transition occurs. The results of spin-polarized calculations are presented in the left column, while the results of nonmagnetic calculations are shown in the right one. Red color denotes the electron-type, while blue color the hole-type surfaces.

gradual decrease of their area, which correlates with the form of the $\text{DOS}(E_F)$ and $\gamma(x)$ dependencies.

4. Magnetic moments from CPA and ordered compound method

As an addition to the presented VCA results obtained for the Co-rich concentrations of the $\text{Y}(\text{Fe}_{1-x}\text{Co}_x)_2$ system, we show the magnetic moments calculated using the coherent potential approximation (CPA) and ordered compound method for a full Co concentration range. The magnetic moments calculated with the CPA and ordered compound methods are shown in Fig. 8. The calculated total magnetic moments are underestimated in comparison to the experimental values [6]. This difference is relatively large and for the intermediate concentrations it is equal to about $0.7 \mu_B \text{ f.u.}^{-1}$.

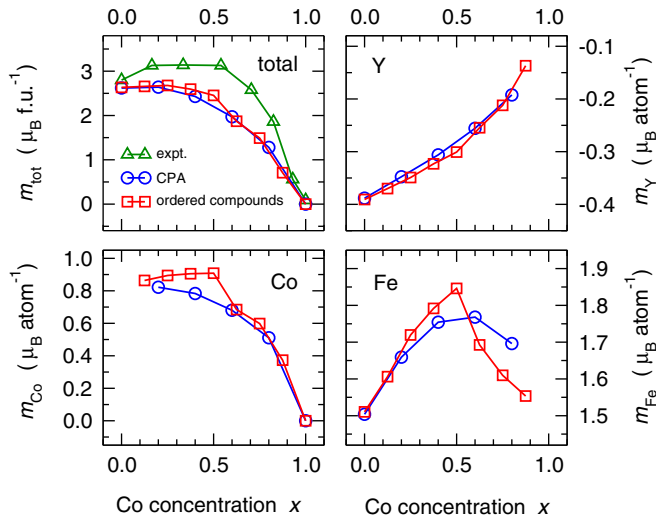


FIG. 8. The spin magnetic moments versus Co concentration x for the $Y(Fe_{1-x}Co_x)_2$ system as calculated with the FPLO-LDA. For YFe_2 and YCo_2 we used optimized lattice parameters and for the intermediate concentrations the lattice parameters obtained using the linear interpolation. The subsequent panels present total magnetic moments and contributions from individual elements. The chemical disorder was treated with the coherent potential approximation (CPA) and the ordered compounds method. The experimental total magnetic moments' dependence comes from the work of Piercy and Taylor [6].

That discrepancy originates, among others, from the limitations of the LDA, which is recognized to underestimate the magnetic moment [48]. Simultaneously, we used the lattice parameters calculated within the LDA (underestimated by about 0.3 Å [7]), which additionally decreased the magnetic moment. The application of the generalized gradient approximation (GGA) gave better values of optimized lattice parameters and magnetic moments, but it overestimated the magnetic energy, leading to a ferromagnetic ground state for YCo_2 and no magnetic phase transition in $Y(Fe_{1-x}Co_x)_2$ was observed [30]. Furthermore, the lattice parameters for the intermediate $Y(Fe_{1-x}Co_x)_2$ concentrations were interpolated assuming a linear behavior of the $a(x)$ dependence, which further decreased the lattice parameters of the intermediate concentrations with respect to the experimental values [7]. Some effect on the calculated magnetic moments has an application of the scalar-relativistic approximation, as a result of which the obtained magnetic moments are completely spin type and do not include the orbital contributions. This deficiency is the magnitude of the orbital moments of the bcc Fe and hcp Co, which have experimental values equal to 0.086 and 0.13 μ_B , respectively [49,50]. The previously observed failure of the LDA + U approach for YCo_2 suggests a necessity to make use of dynamical correlations to improve the theoretical model [30]. However, this goes beyond the scope of this work.

The calculated total magnetic moment for YFe_2 , equal to 2.62 μ_B f.u.⁻¹, is lower than the experimental value of 2.80 μ_B f.u.⁻¹ [6]. The contributions to the total magnetic moment from Fe and Y atoms are equal to 1.51 μ_B and -0.39 μ_B , respectively, in qualitative agreement with the

previous theoretical results (1.68 μ_B and -0.43 μ_B [24]). The calculated spin magnetic moment on Fe in YFe_2 (1.51 μ_B) is reduced in comparison to the measured spin magnetic moment of bcc Fe, equal to 1.98 μ_B [49]. Similarly, the highest values of the magnetic moment on Co in the $Y(Fe_{1-x}Co_x)_2$ system, equal to about 0.8 μ_B on the Fe-rich limit, are significantly reduced with respect to the experimental magnetic moment of fcc Co, equal to 1.67 μ_B [51]. The above picture of the magnetic properties obtained from the CPA and ordered compound method supports the previous findings based on the VCA and helps to better understand the behavior of experimentally observed γ versus x dependence.

IV. SUMMARY AND CONCLUSIONS

In this work we have presented a combined experimental and computational study of the electronic specific heat coefficient γ and magnetic properties of the $Y(Fe_{1-x}Co_x)_2$ Laves phases. For high Co concentrations the measurements indicated the presence of a concentration-induced ferromagnetic-paramagnetic phase transition accompanied by the maximum in γ . The magnetic transition was modeled based on the LDA ground state electronic structure. Calculations showed also that the observed maximum in $\gamma(x)$ results from the presence of the sharp DOS peak on the Fermi level. The LDA-calculated values of γ are significantly underestimated because of not including the many-body effects and spin fluctuations in the LDA description. To improve the calculated γ values we used the so called enhancement factor, introduced and evaluated by another group. The introduction of the enhancement factor let us to incorporate the many-body effects by considering the self-energy of the correlated electrons. Furthermore, in this work another perspective for understanding the formation of the maximum in $\gamma(x)$ was given by simultaneous analysis of magnetic energy and the DOS at the Fermi level as functions of fixed spin moment. Furthermore, using the CPA and ordered compound methods, we calculated the basic magnetic properties of $Y(Fe_{1-x}Co_x)_2$ in the whole range of concentrations.

ACKNOWLEDGMENTS

B.W. and M.W. acknowledge financial support from the Foundation for Polish Science grant HOMING. The HOMING program is cofinanced by the European Union under the European Regional Development Fund. M.W. acknowledges the financial support of the National Science Centre Poland under the decision DEC-2018/30/E/ST3/00267. J.R. acknowledges financial support from the Swedish Research Council. O.E. acknowledges support from the Swedish Research Council, STANUPP, eSENCE, and the KAW Foundation. Some of the computations were performed on resources provided by the Poznań Supercomputing and Networking Center (PSNC).

APPENDIX: CRYSTALLOGRAPHIC DATA OF ORDERED COMPOUNDS

One of the common approximate techniques for a computational treatment of the structures with a chemical disorder is the ordered compound method [25]. It assumes simulating

of a disordered alloy by the ordered compound of the same composition. For example, in the case of the $Y(\text{Fe}_{1-x}\text{Co}_x)_2$ alloys one can represent a Co concentration $x = 0.125$ with an ordered ternary compound $Y_4\text{Fe}_7\text{Co}_1$. The generated structural data of the ordered ternary compounds for x equal 0.125, 0.25, 0.375, and 0.5 are presented in Table III. The other

three intermediate compositions, 0.625, 0.75, and 0.875, can be obtained from the presented data by exchanging atoms on Fe and Co sites. The only free parameter here is the lattice parameter a ; thus these ordered compounds are universal and can be used for calculations of alloys of any AB_2 -type Laves phase.

-
- [1] F. Stein, M. Palm, and G. Sauthoff, Structure and stability of Laves phases. Part I. Critical assessment of factors controlling Laves phase stability, *Intermetallics* **12**, 713 (2004).
- [2] A. Murtaza, S. Yang, T. Chang, A. Ghani, M. T. Khan, R. Zhang, C. Zhou, X. Song, M. Suchomel, and Y. Ren, Spin reorientation and magnetoelastic properties of ferromagnetic $\text{Tb}_{1-x}\text{Nd}_x\text{Co}_2$ systems with a morphotropic phase boundary, *Phys. Rev. B* **97**, 104410 (2018).
- [3] H. Xie, H. Pan, Y. Ren, L. Wang, Y. He, X. Qi, and G. Qin, New Structured Laves Phase in the Mg-In-Ca System with Nontranslational Symmetry and Two Unit Cells, *Phys. Rev. Lett.* **120**, 085701 (2018).
- [4] X. Yan, X.-Q. Chen, H. Michor, W. Wolf, V. T. Witusiewicz, E. Bauer, R. Podloucky, and P. Rogl, Structural, thermodynamic, and electronic properties of Laves-phase NbMn_2 from first principles, x-ray diffraction, and calorimetric experiments, *Phys. Rev. B* **97**, 125110 (2018).
- [5] W. Steiner and H. Ortbauer, Magnetische Messungen an $Y(\text{Fe}_x\text{Co}_{1-x})_2$ im Bereich kleiner Fe-Konzentrationen, *Phys. Status Solidi A* **26**, 451 (1974).
- [6] A. R. Piercy and K. N. R. Taylor, Evidence for an itinerant electron moment in cubic Laves-phase rare-earth-transition-metal compounds, *J. Phys. C: Solid State Phys.* **1**, 1112 (1968).
- [7] P. Guzdek, J. Pszczoła, J. Chmista, P. Stoch, A. Stoch, and J. Suwalski, Electrical resistivity and Mössbauer effect studies of $Y(\text{Fe}_{1-x}\text{Co}_x)_2$ intermetallics, *J. Alloys Compd.* **520**, 72 (2012).
- [8] Y. Yamada and H. Ohmae, NMR study of $Y(\text{Fe}_{1-x}\text{Co}_x)_2$ and $\text{Zr}(\text{Fe}_{1-x}\text{Co}_x)_2$, *J. Phys. Soc. Jpn.* **48**, 1513 (1980).
- [9] K. Schwarz and P. Mohn, Itinerant metamagnetism in YCo_2 , *J. Phys. F: Met. Phys.* **14**, L129 (1984).
- [10] T. Goto, T. Sakakibara, K. Murata, H. Komatsu, and K. Fukamichi, Itinerant electron metamagnetism in YCo_2 and LuCo_2 , *J. Magn. Magn. Mater.* **90-91**, 700 (1990).
- [11] S. H. Kilcoyne, The evolution of magnetic correlations and onset of magnetic order in $Y(\text{Fe}_{1-x}\text{Co}_x)_2$, *Phys. B (Amsterdam)* **276-278**, 660 (2000).
- [12] B. Balamurugan, R. Skomski, X. Z. Li, V. R. Shah, G. C. Hadjipanayis, J. E. Shield, and D. J. Sellmyer, Magnetism of cluster-deposited Y-Co nanoparticles, *J. Appl. Phys.* **109**, 07A707 (2011).
- [13] C. M. Bonilla, D. Paudyal, J. Herrero-Albillos, V. K. Pecharsky, K. A. Gschneidner, L. M. Garcia, and F. Bartolome, Formation of Co moment in the paramagnetic phase of RCo_2 , *IEEE Trans. Magn.* **50**, 1 (2014).
- [14] P. Kumar, A. Kashyap, B. Balamurugan, J. E. Shield, D. J. Sellmyer, and R. Skomski, Permanent magnetism of intermetallic compounds between light and heavy transition-metal elements, *J. Phys.: Condens. Matter* **26**, 064209 (2014).
- [15] V. Paul-Boncour, O. Isnard, M. Guillot, and A. Hoser, Metamagnetic transitions in $\text{Y}_{0.5}\text{Er}_{0.5}\text{Fe}_2\text{D}_{4.2}$ deuteride studied by high magnetic field and neutron diffraction experiments, *J. Magn. Magn. Mater.* **477**, 356 (2019).
- [16] O. Isnard, V. Paul-Boncour, Z. Arnold, C. V. Colin, T. Leblond, J. Kamarad, and H. Sugiura, Pressure-induced changes in the structural and magnetic properties of $\text{YFe}_2\text{D}_{4.2}$, *Phys. Rev. B* **84**, 094429 (2011).
- [17] O. Isnard, V. Paul-Boncour, and Z. Arnold, On the origin of the giant isotopic effect of hydrogen on the magnetic properties of $\text{YFe}_2\text{A}_{4.2}$ ($A = \text{H, D}$): A high pressure study, *Appl. Phys. Lett.* **102**, 122408 (2013).
- [18] Z. Li, H. Wang, L. Ouyang, J. Liu, and M. Zhu, Reversible hydriding in $\text{YFe}_{2-x}\text{Al}_x$ ($x = 0.3, 0.5, 0.7$) intermetallic compounds, *J. Alloys Compd.* **689**, 843 (2016).
- [19] V. Paul-Boncour, M. Guillot, O. Isnard, and A. Hoser, High field induced magnetic transitions in the $\text{Y}_{0.7}\text{Er}_{0.3}\text{Fe}_2\text{D}_{4.2}$ deuteride, *Phys. Rev. B* **96**, 104440 (2017).
- [20] G. B. G. Stenning, G. J. Bowden, P. A. J. de Groot, G. van der Laan, A. I. Figueroa, P. Bencok, P. Steadman, and T. Hesjedal, Exchange spring switching in Er-doped $\text{DyFe}_2/\text{YFe}_2$ magnetic thin films, *Phys. Rev. B* **92**, 104404 (2015).
- [21] X. Fu, B. Warot-Fonrose, R. Arras, K. Dumesnil, and V. Serin, Quantitative moment study and coupling of $4f$ rare earth and $3d$ metal by transmitted electrons, *Phys. Rev. B* **94**, 140416(R) (2016).
- [22] N. V. Baranov, A. V. Proshkin, C. Czernasty, M. Meißner, A. Podlesnyak, and S. M. Podgornykh, Butterflylike specific heat, magnetocaloric effect, and itinerant metamagnetism in $(\text{Er,Y})\text{Co}_2$ compounds, *Phys. Rev. B* **79**, 184420 (2009).
- [23] N. Pierunek, Z. Śniadecki, M. Werwiński, B. Wasilewski, V. Franco, and B. Idzikowski, Normal and inverse magnetocaloric effects in structurally disordered Laves phase $\text{Y}_{1-x}\text{Gd}_x\text{Co}_2$ ($0 < x < 1$) compounds, *J. Alloys Compd.* **702**, 258 (2017).
- [24] O. Eriksson, B. Johansson, and M. S. S. Brooks, Electronic structure and magnetic properties of the $Y(\text{Fe}_{1-x}\text{Co}_x)_2$ alloys, *J. Phys., Colloq.* **49**, C8-295 (1988).
- [25] O. Eriksson, B. Johansson, M. S. S. Brooks, and H. L. Skriver, Electronic structure and magnetic properties of selected lanthanide and actinide intermetallic Laves-phase alloys, *Phys. Rev. B* **40**, 9519 (1989).
- [26] M. Diviš, J. Ruzs, and M. Richter, Electronic structure of RCo_2 ($R = \text{Y, Nd, Ho, Er}$), *Czech. J. Phys.* **52**, 247 (2002).
- [27] J. Ruzs, M. Diviš, and V. Sechovský, Magnetism in RECo_2 compounds under pressure, *J. Magn. Magn. Mater.* **272-276**, E383 (2004).
- [28] Z. Śniadecki, M. Werwiński, A. Szajek, U. K. Röbber, and B. Idzikowski, Induced magnetic ordering in alloyed compounds

- based on Pauli paramagnet YCo_2 , *J. Appl. Phys.* **115**, 17E129 (2014).
- [29] Z. Śniadecki, M. Kopcewicz, N. Pierunek, and B. Idzikowski, Magnetic percolation and inequivalence of Fe sites in $\text{YFe}_x\text{Co}_{2-x}$ ($x = 0.03$ and 1) Laves phase compounds, *Appl. Phys. A* **118**, 1273 (2015).
- [30] B. Wasilewski, W. Marciniak, and M. Werwiński, Curie temperature study of $\text{Y}(\text{Fe}_{1-x}\text{Co}_x)_2$ and $\text{Zr}(\text{Fe}_{1-x}\text{Co}_x)_2$ systems using mean field theory and Monte Carlo method, *J. Phys. D: Appl. Phys.* **51**, 175001 (2018).
- [31] Z. Śniadecki, N. Pierunek, B. Idzikowski, B. Wasilewski, M. Werwiński, U. K. Röbber, and Yu. Ivanisenko, Influence of structural disorder on the magnetic properties and electronic structure of YCo_2 , *Phys. Rev. B* **98**, 094418 (2018).
- [32] E. Gopal, *Specific Heats at Low Temperatures* (Springer Science & Business Media, 2012).
- [33] K. Koepnik, B. Velický, R. Hayn, and H. Eschrig, Self-consistent LCAO-CPA method for disordered alloys, *Phys. Rev. B* **55**, 5717 (1997).
- [34] P. Soven, Application of the coherent potential approximation to a system of muffin-tin potentials, *Phys. Rev. B* **2**, 4715 (1970).
- [35] K. Koepnik and H. Eschrig, Full-potential nonorthogonal local-orbital minimum-basis band-structure scheme, *Phys. Rev. B* **59**, 1743 (1999).
- [36] J. P. Perdew and Y. Wang, Accurate and simple analytic representation of the electron-gas correlation energy, *Phys. Rev. B* **45**, 13244 (1992).
- [37] S. Khmelevskyi, P. Mohn, J. Redinger, and M. Weinert, Magnetism on the Surface of the Bulk Paramagnetic Intermetallic Compound YCo_2 , *Phys. Rev. Lett.* **94**, 146403 (2005).
- [38] W. Zhang and W. Zhang, Collapse of the magnetic moment under pressure of AFe_2 ($A = \text{Y}, \text{Zr}, \text{Lu},$ and Hf) in the cubic Laves phase, *J. Magn. Magn. Mater.* **404**, 83 (2016).
- [39] K. Momma and F. Izumi, VESTA: A three-dimensional visualization system for electronic and structural analysis, *J. Appl. Crystallogr.* **41**, 653 (2008).
- [40] Y. Muraoka, M. Shiga, and Y. Nakamura, Electronic specific heat of $\text{Y}(\text{Fe}_{1-x}\text{Co}_x)_2$, *J. Phys. Soc. Jpn.* **42**, 2067 (1977).
- [41] N. V. Baranov, A. A. Yermakov, and A. Podlesnyak, Onset of magnetism in $\text{Y}_{1-x}\text{Gd}_x\text{Co}_2$: Effect on the heat capacity and electrical resistivity, *J. Phys.: Condens. Matter* **15**, 5371 (2003).
- [42] W. Steiner, Magnetization processes caused by iron substitution in cubic Laves phases, *J. Magn. Magn. Mater.* **14**, 47 (1979).
- [43] K. Terao and M. Shimizu, Spontaneous volume magnetostriction in $\text{Y}(\text{Fe}_{1-x}\text{Co}_x)_2$ and $\text{Zr}(\text{Fe}_{1-x}\text{Co}_x)_2$, *Phys. Lett. A* **95**, 111 (1983).
- [44] H. Yamada, T. Tohyama, and M. Shimizu, Magnetic properties of $\text{Y}(\text{Fe-Co})_2$, *J. Magn. Magn. Mater.* **66**, 409 (1987).
- [45] S. Tanaka and H. Harima, Mass Enhancement Factor and Fermi Surface in YCo_2 , *J. Phys. Soc. Jpn.* **67**, 2594 (1998).
- [46] S. Tanaka, H. Harima, and A. Yanase, Calculations of Fermi surfaces and enhanced electronic specific-heat coefficients in cubic Laves-phase Ce compounds, *J. Phys. Soc. Jpn.* **67**, 1342 (1998).
- [47] G. Hilscher and E. Gratz, An estimation of the density of states from magnetization and resistivity measurements in $\text{Ti}(\text{Fe}_{1-x}\text{Co}_x)$ and $\text{Zr}(\text{Fe}_{1-x}\text{Co}_x)_2$, *Phys. Status Solidi A* **48**, 473 (1978).
- [48] M. Werwiński, A. Edström, J. Ruzs, D. Hedlund, K. Gunnarsson, P. Svedlindh, J. Cedervall, and M. Sahlberg, Magnetocrystalline anisotropy of Fe_5PB_2 and its alloys with Co and $5d$ elements: A combined first-principles and experimental study, *Phys. Rev. B* **98**, 214431 (2018).
- [49] C. T. Chen, Y. U. Idzerda, H.-J. Lin, N. V. Smith, G. Meigs, E. Chaban, G. H. Ho, E. Pellegrin, and F. Sette, Experimental Confirmation of the X-Ray Magnetic Circular Dichroism Sum Rules for Iron and Cobalt, *Phys. Rev. Lett.* **75**, 152 (1995).
- [50] R. M. Moon, Distribution of magnetic moment in hexagonal cobalt, *Phys. Rev.* **136**, A195 (1964).
- [51] R. A. Reck and D. L. Fry, Orbital and spin magnetization in Fe-Co, Fe-Ni, and Ni-Co, *Phys. Rev.* **184**, 492 (1969).